JOURNAL OF CATALYSIS 131, 350–368 (1991)

Catalytic and Spectroscopic Studies of $Ag_{1.2}V_3Ce_yO_{8+x}$ Catalysts for Oxidation of Toluene

ZHI-GUANG YAN[1] AND S. LARS T. ANDERSSON[2]

Department of Chemical Technology, Chemical Center, University of Lund, P.O. Box 124, S-221 00 Lund, Sweden

Received July 20, 1990; revised February 28, 1991

The effects on structure and chemical composition of adding silver and cerium oxide to vanadium oxide catalysts with the general formulae $Ag_{1.2}V_3Ce_yO_{8+x}$, were investigated by measurements with BET, XRD, ESCA, SIMS, and titration of vanadium valence states. These properties were correlated with the catalytic performance in oxidation of toluene. The addition of silver results in multiphasic systems and in a considerably increased V^{4+} concentration of both fresh and used catalysts. The catalysts consist of the β, ε, and δ silver–vanadium oxide bronzes. With reduction during use, x varies from 0 to -0.5 and transformations of these phases occur. The surface is considerably more reduced than the bulk. The degree of reduction of used catalysts increases with the addition of cerium oxide. No cerium phase is identified by XRD for used catalysts, but possibly $CeVO_4$ is present in fresh catalyst. The surface cerium concentration is considerably higher than the nominal bulk composition when Ce/V $\leq$ 0.02, but lower at higher Ce/V ratios. Activity for toluene oxidation increases with the addition of silver. This is also generally the case for cerium oxide additions. However, surface enrichment of cerium upon use at high temperatures gives lower activity. Selectivity for mainly benzaldehyde increases with the addition of silver, while oxidative coupling products are almost absent. Cerium addition further increases selectivity for benzaldehyde and benzoic acid, the latter almost linearly with cerium concentration.

INTRODUCTION

Addition of promoters to vanadium oxide catalysts can increase both activity and selectivity for oxidation of hydrocarbons. Among these, silver oxide has been mentioned in a number of cases for oxidation of aromatic hydrocarbons to phthalic anhydride (*1–8*), oxidation of CO (*9*), and for oxydehydrogenation of alcohols (*10*). It has also been shown that the properties for oxidation of toluene to benzaldehyde is improved by silver additions (*11, 12*). Optimal selectivity for both toluene (*12*) and *o*-oxylene (*6*) oxidation is obtained at about 20–30 at.% silver. The composition of the active phase has not been identified, which is not surprising in view of the fact that Ag_2O and V_2O_5 may form a variety of compounds and bronzes (*13–15*). Three different $Ag_xV_2O_5$ homogeneity regions, the orthorhombic α-phase with $0 < x < 0.01$,the monoclinic β-phase with $0.29 < x < 0.45$, and the monoclinic δ-phase with $0.60 < x < 0.86$, analogous to those present in alkali–vanadium bronzes are known (*15–17*). A fourth homogeneity region, the ε-phase, is obtained at $1 < x < 1.15$ (*17*). Not much is known about homogeneity regions regarding nonstoichiometry in the oxygen content, which plausibly may arise during catalytic operation.

Recently it has been shown that cerium addition can further improve the properties of the V–Ag–O catalyst (*18, 19*). In both cases supported catalysts were studied. In one case the catalyst was prepared by impregnation and with silica as support. It showed good selectivity for benzaldehyde

[1] On leave from Department of Chemical Engineering, East China University of Chemical Technology, P.O. Box 382, 130 Meilong Road, Shanghai 200237, People's Republic of China.

[2] To whom correspondence should be addressed.

0021-9517/91 $3.00

in the absence of steam and to benzaldehyde and benzoic acid in the presence of steam (*18, 20*). In the other case it was prepared from the molten state and with SiC as support and this catalyst also showed an enhanced performance (*19*). Cerium oxide is also a well-known promoter for oxidation catalysts such as molybdates (*21–23*), cobalt oxide (*24*), and precious metals (*25*). For the latter examples the properties for CO_2 production are enhanced whereas for the former, and V–Ag–O catalysts, the selective properties are improved. The effects of cerium oxide additions, in general, and the reason for this apparent contradiction are not well known. Not much is known about the combined system CeO_2–Ag_2O–V_2O_5 except that CeO_2 and V_2O_5 react at high temperatures with formation of $CeVO_4$ (*26*).

The purpose of this study was to investigate the effects of cerium additions on the structure and chemical composition of vanadium–silver oxide catalysts and to correlate these properties with the effects on the catalytic performance in selective oxidation of toluene.

EXPERIMENTAL

The catalysts were prepared by melting mixtures of V_2O_5 (Aldrich Chemie, 99.6%), Ag_2O (BDH, >97%) and CeO_2 (Janssen Chimica, 99.9%) in quartz crucibles at 750°C for 2 h followed by crushing and sieving. The atomic ratio V/Ag was kept constant at 2.5, while the CeO_2 addition was varied. The various catalysts are denoted by their nominal composition, not to be confused with the phase composition. Short form notations such as Ag–V–O, Ag–V–Ce–O, and Ag–V–Ce–X, where x represents the Ce content, are also used.

Activity tests were carried out in a conventional flow microreactor at atmospheric pressure (*27*). The gas, containing 1.3 vol% toluene, 20.0 vol% O_2, and balance N_2, was dosed at a flow rate of 13.7 dm^3h^{-1}. The temperature was varied between 360 and 400°C and in some cases 400–460°C. The reactor contained 1 g catalyst of 100–300 μm particle size mixed with 1 g of inert quartz to avoid adverse thermal effects. The on-line GC analytical method has been described elsewhere (*28*). The reactor was operated isothermally with conversions of 0.1–10%, and the reaction rates were calculated directly from the differential data.

The surface areas were measured with a Micromeritics flowsorb 2300 instrument after degassing at 350°C for 0.5 h.

Chemical analyses of the vanadium valence states were performed by titration with MnO_4^- and Fe^{2+} and with diphenylamine as indicator (*29*). The samples were first dissolved in dilute H_2SO_4 (4 *M*) under heating and stirring for 1.5 h, followed by the addition of some drops of dilute HCl to precipitate AgCl and thereby eliminate any possible interference with Ag^+ during titration. CeO_2 did not dissolve under these conditions.

Secondary ion mass spectroscopy (SIMS) results were obtained with a Kratos XSAM800 PCI SIMS instrument equipped with a Minibeam II ion gun, Balzers 511 quadrupole and charge neutralizer, and using 2-kV Ar^+ and 100-nA ion current.

ESCA measurements were performed on a Kratos XSAM800 instrument. An Al-anode (1486.6 eV) was used. The slitwidth was set at 40° and the analyzer was operated at 40-eV pass energy and at high magnification. Analysis of the spectra was performed with the DS800 data system. No charging effects could be observed for any of the catalysts, and hence no corrections were made. Sensitivity factors were O $1s$ = 1, V $2p_{3/2}$ = 1.86, Ce $3d_{5/2}$ = 6.35, and Ag $3d_{5/2}$ = 4.6. These were obtained by measurements on V_2O_5 (Aldrich Chemie, 99.6%), AgO (BDH, >99), and CeO_2 (Janssen Chimica, 99.9%). The factor for K $2p_{3/2}$ = 1.88 was as supplied by Kratos.

RESULTS

Catalyst Characterisation

Specific Surface Area

The surface areas of the different catalysts are shown in Table 1. The addition of silver to vanadium oxide does not result in

TABLE 1

Surface Area of the Different Catalysts

Catalyst	Surface area (m^2/g)	
	Fresh	Used
V_2O_5	0.36	—
$Ag_{1.2}V_3O_{8+x}$	0.36	0.6
$Ag_{1.2}V_3Ce_{0.03}O_{8+x}$	0.69	0.9
$Ag_{1.2}V_3Ce_{0.06}O_{8+x}$	0.65	0.8
$Ag_{1.2}V_3Ce_{0.15}O_{8+x}$	0.58	0.7
$Ag_{1.2}V_3Ce_{0.18}O_{8+x}$	0.47	0.7
CeO_2	3.32	—

any change in the surface area. Cerium oxide, however, gives an increased surface area with a maximum at about Ce = 0.03–0.06. For all catalysts, slightly larger surface areas were obtained after use in the catalytic reaction.

Bulk Titration

The result of titration for the vanadium valence states is shown in Table 2. Silver-containing catalysts contain an amount of V^{4+}, both before and after reaction, substantially larger than that of V_2O_5. For fresh samples about 7.7% V^{4+} is obtained, which closely corresponds to the composition $Ag_{1.2}V_3O_8$ containing 7.1% V^{4+}. For fresh catalysts the V^{4+} concentration decreases slightly with increasing cerium concentration. After use of the catalysts the V^{4+} concentration increased, an effect which appears larger with higher cerium oxide addition. The degree of reduction is almost doubled after use at high temperatures. In this case the formal composition corresponds closely to $Ag_{1.2}V_3O_{7.5}$ or $Ag_{0.8}V_2O_5$ containing 19% V^{4+}.

XRD Data

The phase composition was studied by X-ray diffraction analysis. The system seems to be mainly constituted of various silver–vanadium bronzes. It was not possible to assign any lines for any of the samples to Ag, any vanadium oxide, CeO_2, Ce_2O_3, or $CeVO_3$.

Table 3 shows data for fresh and used samples of the Ag–V–O catalyst. The main lines occur for fresh Ag–V–O catalyst and used at 320–360°C and 400–460°C at *d*-values between 3.1 and 2.9 Å, which also is the case for the β-, δ-, and ε-phases. In the references, β-$Ag_{0.35}V_2O_5$ (*30*), $Ag_2V_4O_{11}$ (*13, 31*), $Ag_2V_4O_{11-\varepsilon}$ (*30*), and $Ag_{0.68}V_2O_5$ (*32*), only normalized intensity data are given.

TABLE 2

Concentration of Different Vanadium Valence States Determined by Chemical Titration

Catalyst	$V^{x+}/(V^{5+} + V^{4+} + V^{3+})$ (%)					
	Fresh			Used[a]		
	V^{5+}	V^{4+}	V^{3+}	V^{5+}	V^{4+}	V^{3+}
V_2O_5	100.0	0	0	98.0	2.0	0
$Ag_{1.2}V_3O_{8+x}$	91.0	7.7	1.3	84.6	10.3	5.1
$Ag_{1.2}V_3O_{8+x}$[b]				82.4	17.6	0
$Ag_{1.2}V_3Ce_{0.03}O_{8+x}$	93.4	6.6	0	88.4	10.2	1.4
$Ag_{1.2}V_3Ce_{0.06}O_{8+x}$	93.4	6.7	0	88.2	11.0	0.8
$Ag_{1.2}V_3Ce_{0.06}O_{8+x}$[b]				76.6	20.8	2.6
$Ag_{1.2}V_3Ce_{0.15}O_{8+x}$	93.9	6.1	0	88.4	10.4	1.2
$Ag_{1.2}V_3Ce_{0.18}O_{8+x}$	93.9	6.1	0	84.4	15.4	0

[a] Used at low temperature, 320–360°C.
[b] Used at high temperature, 400–460°C.

TABLE 3

X-Ray Powder Diffraction Data for the V–Ag–O Catalyst

As prepared		Used at 320–360°C		Used at 400–460°C		References			
						β^a	ε^b	ε^c	δ^d
d (Å)	I/I_0	d (Å)	I/I_0	d (Å)	I/I_0	I/I_0	I/I_0	I/I_0	I/I_0
3.96	3	3.969	7						
3.843	11	3.884	14	3.870	12	40			
3.761	14	—	tr				70	46	
3.719	21	3.740	11				30	70	
3.548	9	3.583	8	3.55	10				20
3.460	8	3.493	12	3.482	12	12			5
		3.424	14	3.418	9		70	10	
3.378	5	3.361	24			20			
		3.268	6	3.259	26				100
3.209	7	3.222	7						
3.125	8	3.112	26	3.111	17				
3.056	100	3.071	100	3.064	100	100	70	98	
3.020	36	3.034	21	—	tr		60	100	
2.923	23	2.943	21	2.933	60	55	100	52	20
		2.837	5	2.840	8				
2.784	12	2.80	3	2.792	18		80	38	80
2.728	6	2.743	10	2.742	20	38			50
2.676	6						40	10	20
2.557	6	2.569	7	2.561	18				100
2.478	35	2.487	17				40	90	
2.413	5	2.431	8	2.430	13	12			50
2.368	9	2.382	8	2.379	9	12			
2.341	10	2.337	6	2.34	2		70	31	
2.227	7	2.24	2					20	
2.205	10	2.21	3				60	22	
2.168	24	2.178	22	2.175	22	17			
2.013	5						10		
1.979	5	1.99	4	1.97	3	25			50
1.95	2	1.95	2	1.956	8		10	10	80
1.879	9	1.88	4					22	
1.860	6	1.86	4	1.86	7	12	40		
1.841	6	1.84	3	1.835	11		10		
1.808	12	1.814	8	1.815	10	30			
1.794	7						70	14	
1.722	6								
1.682	9	1.69	2	1.69	6			24	

[a] β-$Ag_{0.35}V_2O_5$, Ref. (*30*).
[b] ε-phases, $Ag_2V_4O_{11}$, Ref. (*13, 31*).
[c] ε-phase, $Ag_2V_4O_{11-\varepsilon}$, Ref. (*30*).
[d] δ-phase, $Ag_{0.68}V_2O_5$, Ref. (*32*).

The overall patterns for these phases agree with that for the catalysts, but the d-values deviate somewhat, indicating differences in stoichiometry in Ag and O.

The as-received Ag–V–O catalyst mainly contains β- and ε-phases as indicated in Table 3. For used catalysts the pattern has changed, with shifts in both intensity and line positions. For example, lines at d-values of 3.761, 3.719, 3.020, 2.676, 2.478, 2.341, 2.227, 2.205, and 1.879 Å (all assigned to the ε-phase) have after use of the catalyst

at 320–360°C strongly decreased, while lines at 3.96, 3.46, 3.378, 2.728, and 2.413 Å (all assigned to the β-phase) have increased. Thus, it appears that a mild treatment of the catalysts results in the formation of more β-phase, while the ε-phase decreases. Use of the catalyst at 400–460°C results in further changes in these lines. The appearance of new lines at 3.259 and 2.274 Å and the increased intensity of lines at 3.55, 3.482, 2.933, 2.792, 2.742, 2.561, 2.430, and 1.956 Å indicates formation of a δ-phase, $Ag_{0.68}V_2O_5$, the structure of which has been reported (*32*).

The effect of adding cerium oxide to the catalyst is shown in Tables 4 and 5. Table 4 shows a comparison of fresh catalysts with different concentrations of cerium. The ceri-

TABLE 4

X-Ray Powder Diffraction Data for theV–Ag–Ce–O Catalyst

Ag–V–O		Ag–V–Ce–0.03		Ag–V–Ce–0.06		Ag–V–Ce–0.18		Assign.
d (Å)	I/I_0	d (Å)	I/I_0	d (Å)	I/I_0	d (Å)	I/I_0	
3.96	3	3.933	18	3.936	14	3.946	16	
3.843	11	3.829	13	3.839	11	3.843	18	a
3.761	14	3.758	26	3.761	22	3.769	28	b,c
3.719	21	3.714	34	3.712	24	3.725	38	b,c
		3.66	9	3.663	14	3.687	23	d
3.548	9							
		3.507	43	3.513	39	3.525	36	
3.460	8	3.439	18	3.445	12	3.455	15	a
3.378	5	3.38	3	3.38	2			a
3.209	7	3.200	13	3.206	7	3.20	4	
3.125	8	3.081	63	3.091	36	3.087	63	
3.056	100	3.045	100	3.050	100	3.055	100	a,b,c
3.020	36	3.028	50	3.027	39	3.027	67	b,c
2.923	23	2.925	30	2.923	23	2.929	38	a,b,c
2.784	12	2.780	20	2.780	11	2.787	23	b,c,d
2.728	6	2.725	12	2.735	9	2.742	10	a
2.676	6	2.671	12	2.674	9	2.675	12	b,c
2.557	6	2.578	10	2.576	9	2.57	8	
2.478	35	2.475	42	2.476	35	2.480	45	b,c
		2.440	9	2.440	7	2.448	8	d
2.368	9	2.36	5	2.36	3	2.36	1	a
2.341	10	2.342	41	2.342	32	2.348	41	b,c
2.227	7	2.23	9	2.221	8	2.22	9	c
2.205	10	2.206	16	2.206	9	2.208	14	b,c
2.168	24	2.168	15	2.173	10	2.171	12	a
2.013	5	2.022	12	2.02	8	2.02	7	b
1.979	5	1.971	19	1.972	16	1.975	12	a
1.95	2							b,c
		1.935	8	1.934	6	1.935	8	
1.879	9	1.877	14	1.879	14	1.882	18	c,d
1.860	6	1.86	9	1.86	7	1.859	13	a,b, d
1.841	6	1.838	11	1.838	13	1.843	13	b
1.808	12	1.805	14	1.810	12	1.805	10	a
1.794	7	1.790	14	1.790	11	1.791	13	b,c
1.722	6	1.719	11	1.735	10	1.735	10	d
1.682	9	1.683	13	1.683	9	1.682	11	c

Note. (a) β-$Ag_{0.35}V_2O_5$, Ref. (*30*); (b) ε-phases, $Ag_2V_4O_{11}$, Ref. (*13, 31*); (c) ε-phase, $Ag_2V_4O_{11-\varepsilon}$, Ref. (*30*); (d) $CeVO_4$, tetragonal, Ref. (*33*).

TABLE 5

X-Ray Powder Diffraction Data for the V–Ag–Ce–0.06 Catalyst

As prepared		Used at 320–360°C		Used at 400–460°C		Ref. I/I_0[e]	Assignments
d (Å)	I/I_0	d (Å)	I/I_0	d (Å)	I/I_0		
		4.279	19				
3.936	14	3.971	18	3.967	21		a
3.839	11	3.872	13	3.879	16		b,c
3.761	22	3.786	13				b,c
3.712	24	3.728	20	3.705	41		
3.663	14					100	
		3.576	26	3.570	39		d
3.513	39						
3.445	12	3.475	10	3.473	10		a, d
3.38	2	3.368	34				a
				3.259	49		d
3.206	7						
		3.151	26	3.153	28		
3.091	36						
3.050	100	3.061	100	3.060	100		a,b,c
3.027	39						b,c
2.923	23	2.934	21	2.936	72		a,b,c,d
2.780	11	2.789	9	2.791	31		b,c,d
2.735	9	2.746	11	2.745	39	65	a d
2.674	9	2.68	6				b,c,d
2.576	9	2.600	8	2.60	6	20	a
				2.559	25		d
2.476	35	2.484	19				b,c
2.440	7			2.430	21	6	d
2.36	3	2.379	21	2.377	38		a
2.342	32	2.34	5	2.33	11		b,c
2.221	8	2.22	4				c
2.206	9	2.21	4				b,c
2.173	10	2.174	11	2.175	23		a
2.02	8						b
1.972	16						a, d
				1.953	17	10	b,c,d
1.934	6						
1.879	14	1.891	7				c
1.86	7						a,b
1.838	13			1.834	21		b
1.810	12	1.812	10				a
1.790	11						b,c
1.735	10					2	
1.683	9						c

Note. (a) β-$Ag_{0.35}V_2O_5$, Ref. (*30*), (b) ε-phases, $Ag_2V_4O_{11}$, Ref. (*13, 31*), (c) ε-phase, $Ag_2V_4O_{11-\varepsilon}$, Ref. (*30*), (d) δ-phase, $Ag_{0.68}V_2O_5$, Ref. (*32*), (e) $CeVO_4$, tetragonal, Ref. (*33*).

um-containing samples consist mainly of phases the same as those of the Ag–V–O catalyst. All samples show a main combined line at about 3.0–3.1 Å, consisting of three different lines at about 3.02, 3.05, and 3.08 Å. The last one increases strongly in intensity with the CeO_2 addition. This is also the case for lines at about 3.94, 3.66, 3.51, and 2.44 Å, all of unknown origin. Possibly, the line at 3.663 Å, shifting to 3.689 Å with in-

TABLE 6

Binding Energies[a] and Half-Widths (eV) for Core Levels of Fresh V–Ag–Ce–O Catalysts

Sample	O 1s	V $2p_{3/2}$	Ce $3d_{5/2}$	Ag $3d_{5/2}$
$V_3Ag_{1.2}O_{8+x}$	529.6	516.6	—	367.3
	(1.7)	(2.0)		(1.5)
$V_3Ag_{1.2}Ce_{0.03}O_{8+x}$	529.6	516.6	883.6	367.3
	(1.7)	(1.9)	—	(1.5)
$V_3Ag_{1.2}Ce_{0.06}O_{8+x}$	529.6	516.6	883.6	367.3
	(1.7)	(1.9)	—	(1.5)
$V_3Ag_{1.2}Ce_{0.15}O_{8+x}$	529.6	516.6	883.7	367.2
	(1.7)	(1.9)	—	(1.5)
$V_3Ag_{1.2}Ce_{0.18}O_{8+x}$	529.6	516.6	883.6	367.2
	(1.7)	(1.9)	—	(1.5)
CeO_2	529.0		888.5[b]–882.2	
	(1.5)		(3.5)	
Ag_2O				367.7
				(1.6)
Ag_2O (Ref. (*34*))	529.0			367.7
Ag_2O (Ref. (*35*))	529.2			367.7
AgO (Ref. (*34*))	528.4			367.4
AgO (Ref. (*35*))	528.5			367.3
Ag^0 (Ref. (*34*))				368.1
Ag^0 (Ref. (*36*))				368.2

[a] No charging effects for V–Ag–Ce–O catalysts. CeO_2 and Ag_2O were corrected for charging effects by C $1s$ = 284.5 eV.

[b] Strong satellite.

creased Ce content, is caused by the strongest line of $CeVO_4$ (*33*). Various other lines (see Table 4), could also fit if one allows for small shifts in position by, for example, solid solution of Ag^+ in the $CeVO_4$ phase.

After use of the Ce-containing catalyst, illustrated here with V–Ag–Ce–0.06 (see Table 5), considerable changes occur, some as obtained for the V–Ag–O catalyst. Main effects are that lines for the β-phase increase, lines for the ε-phase decrease, and lines for the δ-phase, $Ag_{0.68}V_2O_5$, appear in catalysts used at high temperatures. Lines possibly due to $CeVO_4$ in as-received catalysts disappear after use.

ESCA Measurements

Fresh catalysts. The surface composition of the catalysts was investigated with ESCA. Binding energies (B.E.) and half-widths for the various core levels are shown in Table 6 for fresh catalysts and in Table 7 for used catalysts. A V $2p_{3/2}$ B.E. of about 516.6 eV for all catalysts indicates the predominance of the pentavalent state of vanadium (*37*).

For the Ag $3d_{5/2}$ line a B.E. of about 367.3 eV is obtained. Comparing with the reference data given in Table 6, it is seen that Ag^0 is not present in any of the fresh catalysts. It is more difficult to make any definite conclusions about the presence of Ag^+ or Ag^{2+} from the Ag $3d_{5/2}$ B.E. data, the difference of which is quite small. However, Ag(II) is an unusual valence state and most stable Ag compounds are based on Ag(I), so we can likely consider a B.E. of 367.3 eV significant for Ag(I). This value, slightly lower than that of Ag_2O, can be caused by the different matrix of Ag(I) when dissolved in the V_2O_5 bronze structures.

Ce $3d$ spectra are quite complex due to various final state effects (*38*). The low cerium concentration prevented these measurements except for the strongest line. This is a broad feature centered at about 883.6

TABLE 7

Binding Energies[a] and Half-Widths (eV) for Core Levels of Used V–Ag–Ce–O Catalysts

Sample	O 1s	V $2p_{3/2}$	Ce $3d_{5/2}$	Ag $3d_{5/2}$
$V_3Ag_{1.2}O_{8+x}$[b]	529.6	516.6	—	367.4
	(1.7)	(2.2)		(1.5)
$V_3Ag_{1.2}O_{8+x}$[c]	529.6	516.6	—	367.4
	(1.7)	(2.5)		(1.5)
$V_3Ag_{1.2}Ce_{0.03}O_{8+x}$[b]	529.6	516.6	883.2	367.3
	(1.8)	(2.1)	—	(1.5)
$V_3Ag_{1.2}Ce_{0.06}O_{8+x}$[b]	529.7	516.6	883.4	367.3
	(1.8)	(2.1)	—	(1.5)
$V_3Ag_{1.2}Ce_{0.06}O_{8+x}$[c]	529.6	516.7	883.4	367.3
	(1.8)	(2.2)	—	(1.5)
$V_3Ag_{1.2}Ce_{0.15}O_{8+x}$[b]	529.6	516.7	883.7	367.4
	(1.7)	(2.3)	—	(1.5)
$V_3Ag_{1.2}Ce_{0.18}O_{8+x}$[b]	529.6	516.6	883.4	367.4
	(1.8)	(2.2)	—	(1.5)

[a] No charging effects.
[b] Used at low temperatures, 320–370°C.
[c] Used at high temperatures, 400–460°C.

eV, which is slightly higher than observed for CeO_2 at 882.2 eV. Due to the complicated origin of the various components, which need not be elaborated here, a slight reduction of CeO_2 at 900°C in H_2 with formation of some Ce^{3+} results in a complex spectrum centered at slightly higher B.E. values (*38*). Thus, our data for the catalysts could possibly be interpreted as a mixture of mainly Ce^{4+} and some Ce^{3+}.

Used catalysts. After use of the catalysts in oxidation of toluene, changes in the ESCA spectra are observed mainly for the V $2p_{3/2}$ core line (see Table 7). The Ag $3d_{5/2}$ line indicates that silver is present as Ag^+ also after use; a difference is not observed for cerium. The changes in the V $2p_{3/2}$ line are mainly seen as an increased half-width caused by reduction of some V^{5+} to V^{4+}. Some representative spectra for fresh and used catalysts as well as difference spectra are shown in Fig. 1. The contribution of both valence states was estimated from difference spectra and by curve synthesis. The latter was done by fitting one component for V^{5+} and one for V^{4+}, at B.E. about 1 eV lower than that of the V $2p_{3/2}$ spectra. Also components for the V $2p_{1/2}$ line and for the O 1*s* line excited by the Al$K\alpha_{3,4}$ satellite are included in the curve-fitting procedure. The results for a representative fresh and a used catalyst are shown in Fig. 2 over the V 2*p* B.E. region. The curve fit is not perfect since the natural and Gaussian curve shapes used are not quite equal. The results of the quantitative estimations of $V^{4+}/(V^4 + V^{5+})$ by curve synthesis and from difference spectra are shown in Table 8. The curve synthesis gives a V^{4+} concentration higher than that given by the difference method. Both methods give a V^{4+} concentration higher than that obtained by chemical titration, as shown in Table 2. This indicates strongly that the surface is more highly reduced than the bulk.

Quantitative analysis. The ESCA data were quantified to obtain elemental ratios and these are presented in Table 9. The data suggest that the surface concentration of silver is slightly higher than the nominal bulk composition. An effect on the surface Ag concentration by the addition of cerium is only observed for catalysts Ag–V–Ce–0.03 and Ag–V–Ce–0.06, giving a lower value.

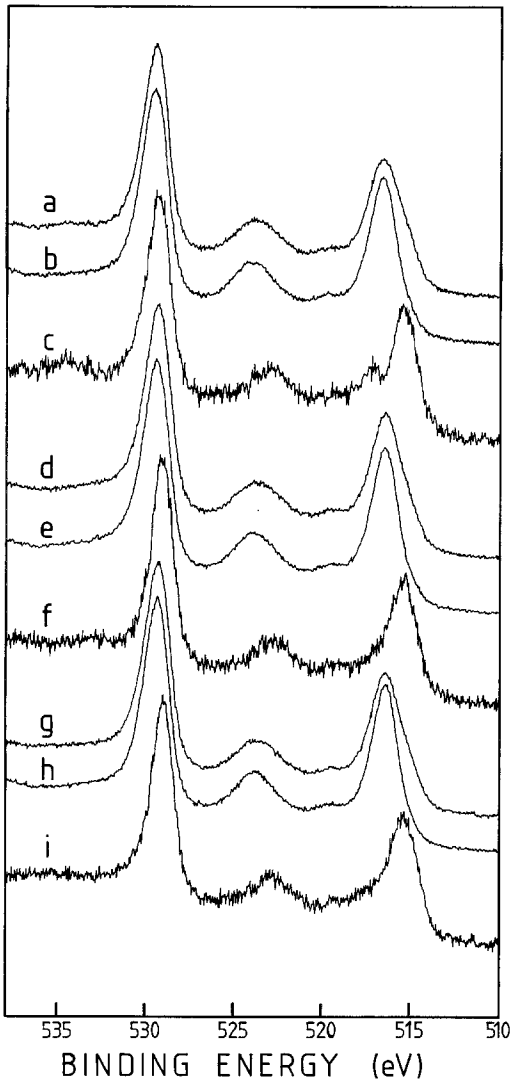

FIG. 1. ESCA spectra of the O 1*s* and the V 2*p* binding energy region of some fresh and used $Ag_{1.2}V_3Ce_yO_{8+x}$ catalysts with different cerium content, *y*. (a) $y = 0$, used at 320–370°C; (b) $y = 0$, Fresh; (c) difference spectrum, (a)–(b); (d) $y = 0.06$, used at 320–370°C; (e) $y = 0.06$, fresh; (f) difference spectrum (d)–(e); (g) $y = 0.18$, used at 320–370°C; (h) $y = 0.18$, fresh; (i) difference spectrum, (g)–(h).

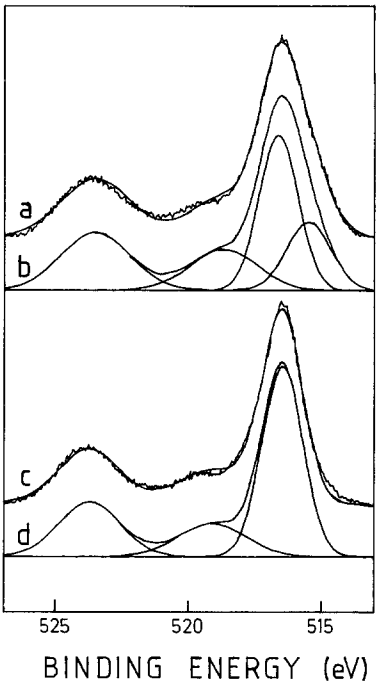

FIG. 2. ESCA spectra of the V 2*p* binding energy region of used and fresh $Ag_{1.2}V_3Ce_{0.18}O_{8+x}$ catalyst resolved in components by curve synthesis. (a) Natural and synthetic envelope for used catalyst; (b) synthetic envelope and Gaussian components for used catalyst; (c) natural and synthetic envelope for fresh catalyst; (d) synthetic envelope and Gaussian components for used catalyst.

However, by using the catalysts at low temperature a decreased surface silver concentration results.

The surface cerium concentration as obtained by ESCA is larger than the nominal bulk concentration at cerium stoichiometry up to 0.06 (see Table 9). At higher cerium additions, the surface concentration is lower than the bulk. Figure 3 shows the Ce/V atom ratio by ESCA as a function of the nominal bulk ratio. Also included in the figure are data for used catalysts and it is evident that for these even higher Ce/V ratios are obtained.

The O/V ratio, also given in Table 9, is for several of the fresh catalysts close to the nominal values, and upon use decreased values are obtained because of the reduction of pentavalent vanadium to tetravalent vanadium with concomitant oxygen loss. The oxygen content corrected for the amount of V^{4+} according to the chemical titration is also given in Table 9. Excessive O/V values by ESCA indicate surface segregation of cerium compounds.

TABLE 8

Binding Energies and Half-Widths (eV) for V $2p_{3/2}$ Obtained by Curve Synthesis of Spectra for Used V–Ag–Ce–O Catalysts

Sample	V $2p_{3/2}$		$V^{4+}/(V^{4+} + V^{5+})$ (%)	
	V^{4+}	V^{5+}	Curve synthesis	Difference spectra
$V_3Ag_{1.2}O_{8+x}$[a]	516.0 (2.4)	516.7 (2.0)	38	15
$V_3Ag_{1.2}O_{8+x}$[b]	515.9 (2.5)	516.8 (2.2)	40	24
$V_3Ag_{1.2}Ce_{0.03}O_{8+x}$[a]	516.0 (2.4)	516.7 (1.9)	34	23
$V_3Ag_{1.2}Ce_{0.06}O_{8+x}$[a]	516.0 (2.5)	516.7 (1.9)	36	19
$V_3Ag_{1.2}Ce_{0.06}O_{8+x}$[b]	515.9 (2.4)	516.7 (1.9)	34	24
$V_3Ag_{1.2}Ce_{0.15}O_{8+x}$[a]	515.9 (2.4)	516.8 (2.0)	34	28
$V_3Ag_{1.2}Ce_{0.18}O_{8+x}$[a]	515.9 (2.0)	517.0 (1.8)	36	36

[a] Used at low temperatures, 320–370°C.
[b] Used at high temperatures, 400–460°C.

SIMS Measurements

The catalysts were also investigated by SIMS and the results are presented in Fig. 4. The positive ion spectra mainly contained peaks for V^+, VO^+, V_2^+, $V_2O_2^+$, Ag^+, Ce^+, and CeO^+, and the only combined peak detected was for AgV^+. The latter is an indica-

TABLE 9

Composition of $Ag_{1.2}V_3Ce_yO_{8+x}$ Catalysts as Measured by ESCA

Ce content, y	Atom ratios[a]				O/3V	
	V	Ag	Ce	O	Nomin.	Calc[b]
0, Fresh	3	1.41	0	7.89	8.10	7.95
0, Used[c]	3	1.36	0	6.98	8.10	7.79
0, Used[d]	3	1.36	0	6.97	8.10	7.84
0.03, Fresh	3	1.27	0.053	8.08	8.16	8.06
0.03, Used[c]	3	1.22	0.067	7.84	8.16	7.97
0.06, Fresh	3	1.31	0.11	8.55	8.22	8.12
0.06, Used[c]	3	1.27	0.13	8.15	8.22	8.03
0.06, Used[d]	3	1.35	0.15	8.41	8.22	7.83
0.15, Fresh	3	1.40	0.12	8.20	8.40	8.31
0.15, Used[c]	3	1.31	0.16	7.88	8.40	8.21
0.18, Fresh	3	1.41	0.12	8.23	8.46	8.37
0.18, Used[c]	3	1.36	0.10	8.29	8.46	8.23

[a] The base for ratios is V = 3 as in the stoichiometric formulae.
[b] The calculation is based on the amount of V^{3+} and V^{4+} as determined by the chemical titration.
[c] Used at low temperatures, 320–370°C.
[d] Used at high temperatures, 400–460°C.

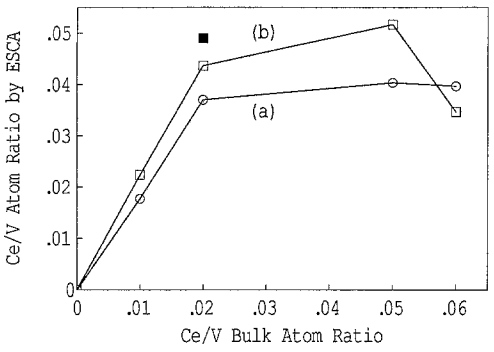

FIG. 3. The Ce/V atom ratio determined by ESCA analysis as a function of the nominal bulk composition. (a) Fresh catalyst; (b) catalyst used at 320–370°C. Solid symbol denotes catalyst used at 400–470°C.

tion of the proximity of Ag and V ions in the bronzes. Main contaminations found by SIMS were potassium and sodium. Low concentrations of the former were also identified by ESCA analysis. From the $(^{140}Ce^+ + {}^{142}Ce^+ + {}^{156}CeO^+ + {}^{158}CeO^+)/{}^{51}V^+$ intensity ratio as a function of nominal bulk Ce/V atom ratio, presented in Fig. 5, it is seen that a constant cerium concentration appears to have been obtained at above Ce/V = 0.06, as also found in the ESCA analysis. The $({}^{107}Ag^+ + {}^{109}Ag^+)/{}^{51}V^+$ and the $^{16}O^-/{}^{51}V^+$ intensity ratios, as a function of the Ce/V bulk atom ratio, show a maximum at Ce/V = 0.06.

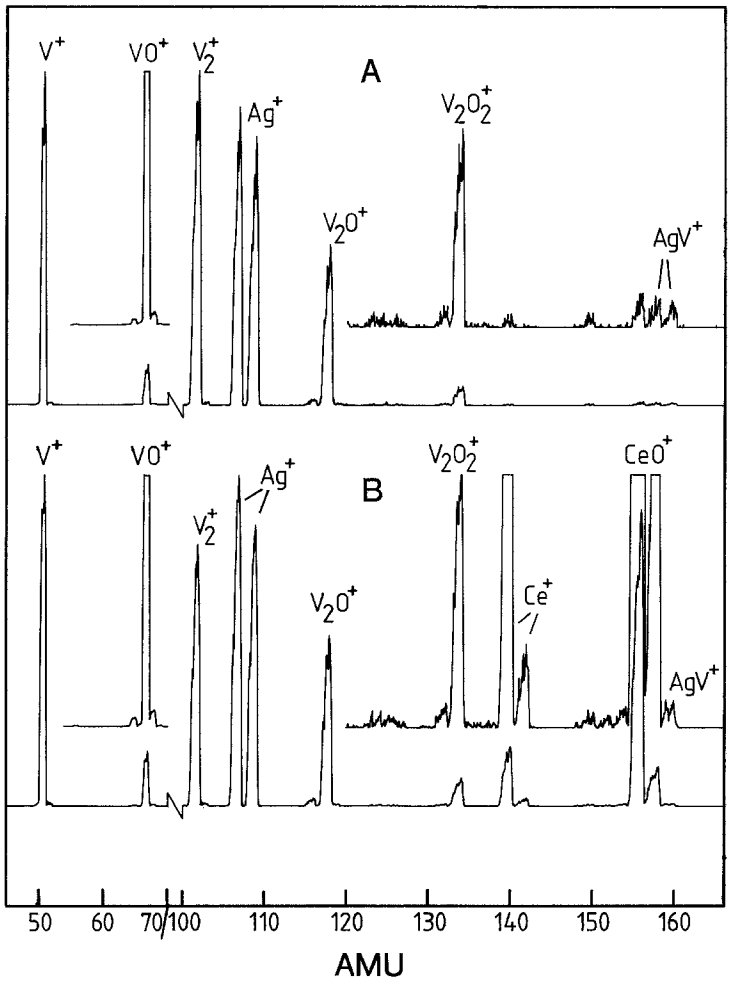

FIG. 4. SIMS spectra for some $Ag_{1.2}V_3Ce_yO_{8+x}$ catalysts. (a) $y = 0$; (b) $y = 0.06$. (Inserts are magnified ×10. AMU region 100–170 is in (a) magnified 265× and in (b) magnified 202×.)

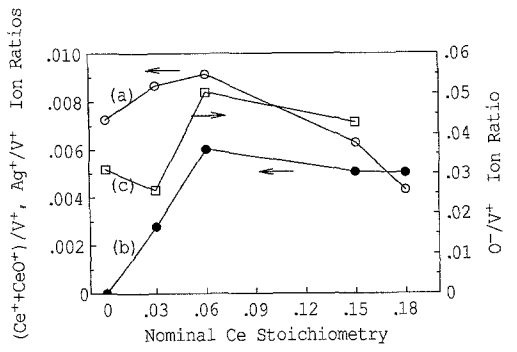

FIG. 5. Some peak intensity ratios obtained from SIMS spectra for $Ag_{1.2}V_3Ce_yO_{8+x}$ catalysts. (a) ($^{107}Ag^+ + {}^{109}Ag^+)/{}^{51}V^+$; (b) ($^{140}Ce^+ + {}^{142}Ce^+ + {}^{156}CeO^+ + {}^{158}CeO^+)/{}^{51}V^+$; (c) $^{16}O^-/{}^{51}V^+$.

CATALYTIC PROPERTIES

Activity Measurements

The rate of oxidation of toluene at 370°C over the different catalysts is shown in Fig. 6, both as activity per gram and per square meter. In both cases the rate over the vanadium oxide used is considerably increased by the introduction of silver. The addition of cerium also increases the rate per gram of catalyst. However, the rate per square meter shows a minimum at low cerium concentration. Rates based on surface areas measured after use give essentially the same result. The rate for oxidation of toluene over CeO_2 is lower than that for any of the $Ag_{1.2}V_3Ce_yO_{8+x}$ catalysts, but considerably higher than that for the V_2O_5 catalyst.

Arrhenius plots of the rate data showed that for $Ag_{1.2}V_3Ce_yO_{8+x}$ catalysts at temperatures of 320–370°C almost parallel lines are obtained, giving apparent activation energies of about 164 ± 5 kJ/mole. The increased rate with increased Ce content corresponds with an increase in the preexponential factor from 1.3×10^{12} to 1.1×10^{14}, suggesting that the rate increase is caused mainly by an increase in the number of active sites.

The behavior is quite different at temperatures as high as 400–460°C, where the rate over $Ag_{1.2}V_3O_{8+x}$ increases considerably more than the rate over the cerium-promoted catalyst $Ag_{1.2}V_3Ce_{0.06}O_{8+x}$. This is probably due to the pronounced structural changes at high temperatures, as shown above. Therefore no attempts were made to derive Arrhenius parameters from these data.

Selectivity Measurements

Selective oxidation of toluene occurs mainly along parallel reaction routes of side-chain oxidation and oxidative coupling (*39–41*). Selectivities to benzaldehyde (BA), benzoic acid (BzA), the side-chain oxidation products (including BA and BzA), and oxidative coupling products are shown in Fig. 7 as a function of the cerium content of $Ag_{1.2}V_3Ce_yO_{8+x}$ catalysts. The figure also includes data for CeO_2 and V_2O_5.

CeO_2. This pure oxide gives total combustion almost exclusively; selective oxidation products benzene (B), benzaldehyde, methyl-diphenylmethane (MDPM), and *o*-methyl-diphenylmethanone (*o*-MDPM) together amounted to less than 0.8%.

V_2O_5. The V_2O_5 catalyst used, melted and well crystallized, gives a selectivity for side-chain oxidation products of 30% and of oxidative coupling products of 29%. The side-

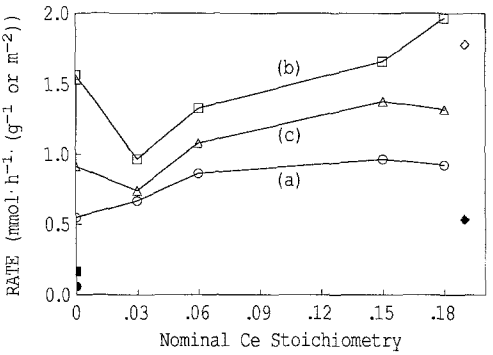

FIG. 6. Rate of toluene oxidation over $Ag_{1.2}V_3Ce_yO_{8+x}$ at 370°C. (a) Rate per gram of catalyst; (b) rate per square meter of catalyst. Surface area measured on fresh catalysts; (c) rate per square meter of catalyst. Surface area measured on used catalysts. Rates over V_2O_5; (●) per gram of catalyst, (■) per square meter. Rates over CeO_2; (◇) per gram of catalyst, (◆) per square meter.

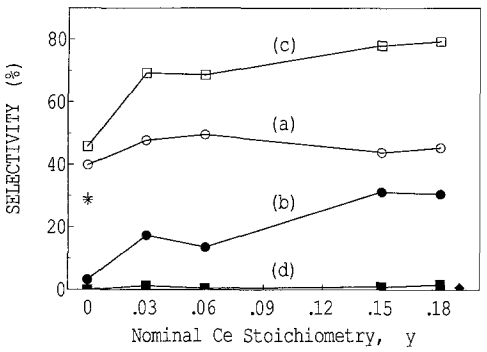

FIG. 7. Selectivity of toluene oxidation over $Ag_{1.2}V_3Ce_yO_{8+x}$ at 370°C. (a) Benzaldehyde (BA); (b) benzoic acid (BzA); (c) side-chain oxidation products, including BA and BzA; (d) oxidative coupling products. Selectivities over V_2O_5: (*) Benzaldehyde and (+) oxidative coupling products. Selectivities over CeO_2: (◆) Sum of selective products.

chain oxidation products are dominated by benzaldehyde, 28.5%, and benzoic acid, 1.5%, while remaining products, benzoquinone (BQ) and maleic anhydride (MA) are low. The oxidative coupling products are mainly phthalic anhydride (PA), MDPM, *o*-MDPM, *p*-methyl-diphenylmethanone (*p*-MDPM), diphenyl-ethanedione (DPED), and anthraquinone (AQ).

Ag–V–O. The introduction of silver to the vanadium oxide, catalyst $Ag_{1.2}V_3O_{8+x}$, results in an almost complete disappearance of the coupling products, traces of PA being detected only (see Fig. 7). The sum of selective products has decreased from 60% for V_2O_5 to 46% for $Ag_{1.2}V_3O_{8+x}$, but benzaldehyde selectivity has increased from 29 to 40%. The introduction of silver to the system also results in the appearance of benzene as a product and a small increase in selectivity for BzA.

Ag–V–Ce–O. The addition of CeO_2 to the $Ag_{1.2}V_3O_{8+x}$ catalyst gives a strongly increased selectivity for side-chain products, i.e., up to as much as 80% (see Fig. 7). The main increase is in BzA with less in BA, while coupling products are almost negligible, around 1%. The selectivity for BzA increases with decreasing temperature. It is known (*42*) that benzoic acid decomposes homogeneously above 370°C at atmospheric pressure, but the rate is many orders of magnitude lower than that required to explain this effect. However, in oxidation of benzaldehyde over V_2O_5, a similar temperature dependence of the selectivity for benzoic acid was obtained (*41*). This dependence is due to its further catalytic oxidation to carbon oxides.

Mixed product feed. Experiments with oxidation of a mixed product feed were performed with two catalyst beds in series. The first bed, upstream, consisted of the V_2O_5 catalyst producing an outlet feed containing all the various products. This bed was followed by a second catalyst bed, downstream, consisting of one of the catalysts $Ag_{1.2}V_3O_{8+x}$ or $Ag_{1.2}Ce_{0.06}V_3O_{8+x}$. Thus, it is possible to follow the conversion of the various products over each one of these catalysts by comparing overall yields.

Figure 8 shows the conversion of toluene and the yield of products of the three main routes, i.e., carbon oxides, side-chain oxidation products, and oxidative coupling

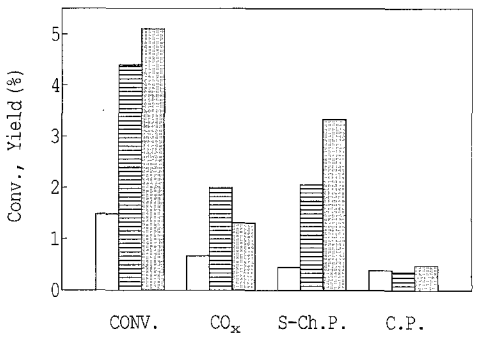

FIG. 8. Comparison of oxidation of mixed product feed over V_2O_5, $Ag_{1.2}V_3O_{8+x}$ and $Ag_{1.2}V_3Ce_{0.06}O_{8+x}$ catalysts. Conversion of toluene and yield of carbon oxides (CO_x), side-chain oxidation products (S-Ch.P.) and oxidative coupling products (C.P.). Blank bars; single bed, 2.0 g V_2O_5. Horizontal lined bars; two beds, first bed 2.0 g V_2O_5 followed by a second bed of 0.4 g $Ag_{1.2}V_3O_{8+x}$. Speckled bars; two beds, first bed 2.0 g V_2O_5 followed by a second bed of 0.4 g $Ag_{1.2}V_3Ce_{0.06}O_{8+x}$.

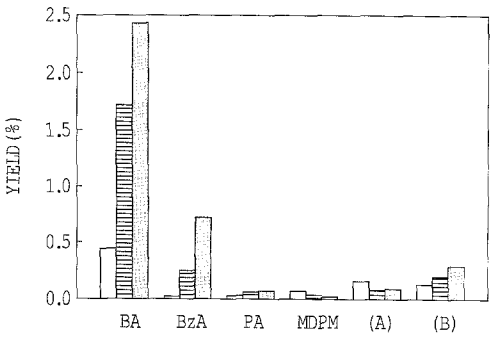

FIG. 9. Comparison of oxidation of mixed product feed over V_2O_5, $Ag_{1.2}V_3O_{8+x}$ and $Ag_{1.2}V_3Ce_{0.06}O_{8+x}$ catalysts. Yield of (BA) benzaldehyde, (BzA) benzoic acid, (PA) phthalic anhydride, (MDPM) methyl-diphenylmethane. (A) Sum of biphenyl-methanone (BPM), *o*-methyl-diphenylmethanone (*o*-MDPM) and *p*-methyl-diphenylmethanone (*p*-MDPM). (B) Sum of diphenyl-ethanone (DPE), diphenyl-ethandione (DPED), and anthraquinone (AN). Bar definitions as in Fig. 8.

products. Clearly, in this experiment, the conversion of toluene over the second bed is considerable, compared with the first bed, and effects on product oxidation, if important, should appear. Thus, catalyst containing silver as the second bed, gives an almost negligible effect on the sum of the yield of coupling products. For catalysts that also contain cerium, a small increase in the sum of coupling products is observed, due to a small activity for formation of these. Neither of these catalysts, therefore, produces or facilitates combustion of coupling products.

Figure 9 shows yields of products and product groups, mainly concerning the coupling products. The promoting effect of cerium for benzaldehyde and benzoic acid formation is evident. The sum of coupling products is hardly affected by the silver and cerium additions, but there are changes within this group seen by decreased yields of MDPM and (A). Thus, these additions do facilitate oxidation of the hydrocarbons, toluene, MDPM, and the methanone products as summed in group (A), consisting of methyl substituted and nonsubstituted diphenyl-methanones (biphenyl-methanone (BPM), *o*-methyl-diphenylmethanone, and *p*-methyl-diphenyl-methanone). Due to oxidation of these products, with the exceptions BPM and *p*-MDPM that give primary products belonging to the side-chain oxidation route (*41*), other more oxidized coupling products summed in (B) and phthalic anhydride occur in higher yield. This group (B) consists of diphenyl-ethanone (DPE), diphenyl-ethanedione and anthraquinone (AN) and these are apparently not combusted over catalysts with silver and cerium additions.

DISCUSSION

Catalyst Composition and Structure

Effects of Ag_2O addition. The catalysts were prepared from Ag_2O, V_2O_5, and CeO_2 by melting at 750°C in air. Under these conditions it is known that CeO_2 and V_2O_5 react with formation of tetragonal $CeVO_4$ (*26*), whereas Ag_2O and V_2O_5 may form a variety of compounds and bronzes (*13–15*). Referring to $Ag_xV_2O_5$ stoichiometry, the present catalysts have a composition corresponding to $x = 0.8$, i.e., close to the upper limit of the δ-phase region. There is no information concerning reactions for the complete system, but it may be interesting to consider published phase diagrams for parts of the system. For Ag_2O–V_2O_5 in oxygen (*13*), it appears that the phases formed during solidification are $Ag_2V_4O_{11}$, belonging to the ε-phase, and AgV_7O_{18}. For Ag_2O–V_2O_5 in air the ε-phase is also formed although the phase diagram appears different (*14*). The second phase, however, was identified as the β-phase $Ag_{0.35}V_2O_5$. This phase was also found for Ag–V_2O_5 in vacuum (*15*).

The results from the present study show that the $Ag_{1.2}V_3O_8$ catalyst is multiphasic, initially consisting of several silver vanadium bronzes, i.e., the β-phase and ε-phase mainly. The main valence states identified by ESCA are Ag^+ and V^{5+}, although these catalysts contain about 7% V^{4+} as determined by titration. The ESCA data suggest that the surface Ag concentration is slightly

higher than nominal. The surface composition probably reflects the heterogeneous distribution of phases of different silver content and particle sizes, but surface segregation cannot be excluded.

The use of the catalyst at low temperatures (320–370°C) results in changes in the phase composition. These are probably induced by oxygen loss due to reduction of the materials during use, which also results in a small increase in the surface area. Titration indicates a small increase to about 10% V^{4+}, whereas by ESCA a considerable surface reduction appears with formation of about 15–35% V^{4+}. Silver is still identified as Ag^{+} and its surface concentration has decreased. These differences may be connected with the changes in the phase composition, i.e., an increased amount of the β-phase and decreased ε-phase.

Use of the catalyst at high temperatures (400–460°C) results in a further increase in the β-phase and decrease in the ε-phase, but also in the appearance of lines suggesting formation of the δ-phase $Ag_{0.68}V_2O_5$. The mean valence state, as determined by titration, corresponds to an overall composition of $Ag_{0.8}V_2O_5$ or $Ag_{1.2}V_3O_{7.5}$ after use at high temperature. Although the V^{4+} concentration by titration has almost doubled from 10 to 20% V^{4+}, the surface V^{4+} concentration by ESCA has only changed marginally. The presence of the β-, ε-, and δ-phases has been reported earlier (*6, 10, 12*), but we do not find specific compounds of composition $Ag_{1.12}V_3O_7$ or $Ag_{1.2}V_3O_8$, nor can we identify any metallic Ag, as suggested elsewhere (*10–12*). The latter difference may depend on the considerably higher silver concentration used in those studies, but perhaps more important, considerably more reducing environment with higher hydrocarbon partial pressure.

The initial presence of β- and ε-phases is mainly in accordance with decomposition of the δ-phase into the β- and ε-phases (*17*) during catalyst preparation. The reappearance of a δ-phase after high temperature use, where the catalyst is considerably reduced, is interpreted on the basis that the reversed reaction is possible under reducing conditions, i.e.,

$$2\beta + \varepsilon \rightarrow 4\delta + \tfrac{1}{2} \cdot O_2,$$

which almost exactly fits the Ag stoichiometries in $Ag_{0.35}V_2O_5$ and $Ag_{0.68}V_2O_5$. Considering that the surface reduction determined by ESCA is higher than the bulk reduction, as determined by titration, it is reasonable to assume that this reaction is complete in the surface layer. Furthermore, since surface reduction of low- and high-temperature used catalysts is similar, this probably holds for all used catalysts.

Effects of CeO_2 additions. The $Ag_{1.2}V_3Ce_yO_{8+x}$ catalysts are also multiphasic systems, initially consisting of several silver vanadium bronzes, the β-phase and ε-phase mainly. The only difference from the Ag–V–O catalyst is the presence of some $CeVO_4$ as analyzed with XRD. It should be emphasized that this identification was not definite and there are also unidentified lines, possibly due to the presence of some other cerium compound. Both ESCA and SIMS data show that the surface Ce concentration is considerably higher than nominal, at Ce/V $\leq$ 0.02, whereas at higher Ce/V ratios, values lower than nominal are obtained. These appear almost constant above Ce/V = 0.02, so additional quantities do not change the surface coverage much. The data may indicate that at low concentration the cerium compounds are highly dispersed on the surface of the silver–vanadium bronze. This is in correspondence with a decrease in the Ag/V ratio by ESCA in this concentration range. At higher cerium concentration, the reversed situation indicates a lower dispersion of the cerium phase, possibly of a different composition.

The phase transformations occurring in the bronze phases of the cerium-containing catalysts during use are similar to those obtained for the Ag–V–O catalyst. All lines ascribed to $CeVO_4$, initially present, have disappeared after use and any Ce-containing phase could not be identified in used cata-

lysts. With ESCA analysis Ag^+ is still present, and increased amounts of V^{4+} are found, apparently higher at higher cerium concentration. ESCA data show a decreased Ag and increased Ce surface concentration, and apparently the $CeVO_4$ initially present forms better dispersed amorphous surface phases upon reduction of the catalyst. Since the surface then is better covered, Ag intensities decrease. Also the increased concentration of the β bronze, after use, suggests a decreasing Ag concentration. The further transformations during use at high temperatures is as described for the Ag–V–O catalyst, namely appearance of XRD lines for the δ-phase, $Ag_{0.68}V_2O_5$.

One obvious and important effect of the CeO_2 addition is a considerable increase in surface area. This is largest at the lowest concentration of cerium oxide. It may be caused by a different crystallization behavior upon solidification during preparation because of the impurity present. The surface area of CeO_2 alone, assuming it is a separate phase, could not contribute more than 0.04 m^2/g to this sample, if calculating with the surface area of the original CeO_2.

Model surfaces. It seems reasonable to assume that the various phases detected are present at the surface as well as in the bulk. The crystal structures of these phases are not all known. The β bronze is isotypic with the alkali β bronzes (*16*). The structure consists of three distinct distorted VO_6 octahedra sharing edges and corners, two forming double chains interconnected by the third. The dodecahedral spaces forming a tunnel structure may hold two Ag^+ ions, mainly coordinated to the double-bonded oxygens of the VO_6^- octahedra. In the δ-phase, $Ag_{0.68}V_2O_5$, the structure also consists of distorted VO_6-octahedra sharing edges and corners, but forming double layers (*32*). The Ag atoms are placed between the layers in positions of fivefold coordination with the double-bonded oxygens of the VO_6 octahedra. Also notable is that the V=O distances are about 1.49 and 1.54 Å, slightly shorter than 1.585 Å for V_2O_5 (*43*). The crystal structure of the ε-phase is not known, but the structure is possibly built up in a similar way with Ag^+ coordinated to mainly double-bonded oxygens. The structure of the working catalyst is thus rather complex, but contains as essential elements distorted VO_6-octahedra with V=O bonds shorter than in V_2O_5 and Ag^+ ions coordinated to the V=O oxygens. As a first approximation we may assume that the situation at the surface is similar to that in the bulk, and contains V=O species, both coordinated to Ag^+ ions and due to a fractional occupancy of its site, also uncoordinated V=O species. Figure 10

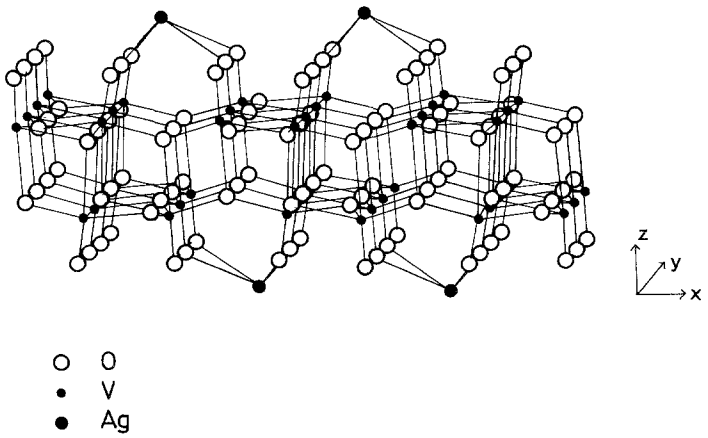

FIG. 10. Structure of $Ag_{0.68}V_2O_5$.

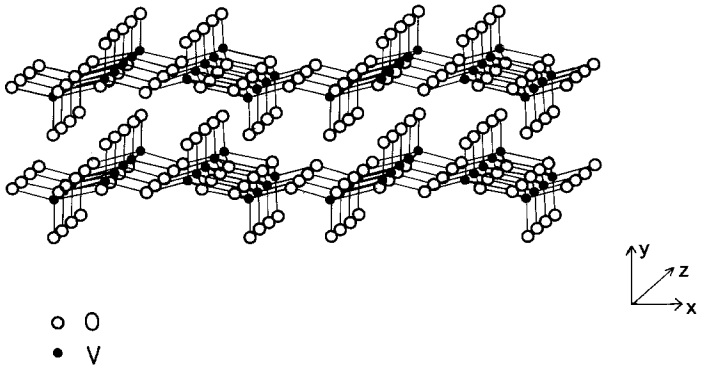

FIG. 11. Structure of V_2O_5.

shows such a possible surface configuration. An important difference from the structure of V_2O_5 concerns the (010) plane exposing arrays of V=O and V^{5+}-cations (see Fig.11). It is thought that these structural differences can explain the various catalytic properties.

Catalytic Performance in Relation to Structure

V–Ag–O catalyst. The catalytic effects of the addition of Ag are an increased selectivity for side-chain oxidation products and a complete lack of oxidative coupling products (CP). The activity per unit surface area also increases considerably. Experiments on oxidation of a mixed product feed showed that an increased part of initial intermediates reacts toward side-chain oxidation in preference over oxidative coupling, explaining the lack of coupling products.

The effects can be rationalized on the basis of the structural differences (see Figs. 10 and 11). Earlier observations suggest that formation of the CP is enhanced over well-crystallized V_2O_5 (*44, 45*) containing a considerable fraction of exposed (010) crystal planes, whereas amorphous and highly dispersed V_2O_5 produces much less CP, if any (*46*). An important ingredient for their formation is thought to be surface properties such as production of the initial intermediates at high concentration and facilitation of their interaction. This situation may arise at the (010) plane where arrays of V=O species and V^{5+} cations are exposed (see Fig. 11). In the initial adsorption step of toluene, a coordination of the ring system to the cations could activate the molecule for the subsequent step. A partial or full charge-transfer would considerably reduce the methyl-hydrogen bond energy, greatly facilitating the hydrogen abstraction process (*40*). The latter function is fulfilled by the strongly nucleophilic V=O oxygen, and for geometric reasons, may occur while the molecule is still coordinated to the cation center. The reaction may continue along two directions; either the intermediate is retained on the cation center or else it reacts with another V=O oxygen. In the last case further reactions lead to benzaldehyde and benzoic acid. In the former case, encounter with a second intermediate or molecule leads to coupling products.

Based on this model, one may account for the effect of the Ag addition with the structure of the δ-phase. In this surface (see Fig. 10), coordinatively unsaturated Ag^+ ions are present, bonded to V=O oxygens. Depending on the Ag content of the phase, these sites will be only partially occupied, and both Ag^+ ions and V=O species are available for the reaction. The Ag^+ ions may take the role of the coordination center, while the V=O oxygens are of a higher nucleophilicity than in V_2O_5, as seen by the shorter bond length. This combined effect

could explain the increased activity of the Ag–V–O catalyst and the increased tendency for side reactions of the intermediate. Since the Ag sites are dispersed over the surface, it is considered less probable that the intermediate encounters a second intermediate or molecule for formation of CP. Rather, a higher probability for continued reaction with a second V=O species for further reactions along the side-chain reaction route is considered.

The model discussed above does not consider irregularities such as defects and partially reduced phases. The activity of the β-phase for oxidation of CO has been discussed in terms of defects as in V_2O_5 (*9*). Clearly, one effect of the Ag-addition is to raise the concentration of V^{4+} (see Table 2). The higher reactivity of the β-phase is also seen as an increased rate of reduction by H_2 and a lowered onset temperature (*47*). Also a facilitated lattice oxygen desorption was observed (*48*). The effects suggest a combination of increased hydrogen abstraction strength with increased mobility of lattice oxygen.

Ag–V–Ce–O catalysts. The catalytic effect of Ce is mainly to increase the selectivity, which is as high as 80% for side-chain products.The main promoting effect is for benzoic acid, whereas benzaldehyde has increased less. A certain activity for formation of some oxidative coupling products are observed. The increased selectivity is opposed to the completely unselective properties of CeO_2 itself, which indicates that any free CeO_2 is not present in the catalyst. The activity of the material is also affected. With cerium addition to the Ag–V–O catalyst, activity increases, except at low concentrations, where lower activity is obtained.

The effects of cerium are not easily interpreted on a structural basis. Possibly a model with cerium compounds partly dispersed on the surface of the active silver–vanadium bronzes could be useful. Then the activity drop at low cerium concentration can be correlated with a partial coverage by less active cerium compounds. In support of this, a further surface segregation of cerium by use of catalysts at high temperatures results in a decreased selectivity, and CeO_2 was found to be less active than the Ag–V–O catalyst. The increased rate at higher concentration is possibly correlated with a decreased cerium dispersion, resulting in less coverage. The Ce concentration should consequently fall within a suitable range.

The dispersion effects of the cerium compounds over the surface are not clearly conceivable, and one should also consider effects of a close proximity between Ce^{3+}/Ce^{4+} redox couples and the active site. The Ce^{3+}/Ce^{4+} redox component was considered important for maintaining the activity of Bi–Mo and Te–Mo oxide catalysts for ammoxidation of propylene by promoting rapid reoxidation and reconstruction of the active sites (*21*). In exhaust cleaning catalysts, cerium oxide has frequently been considered as an oxygen storage function (*25, 49*). It has, however, become recognized that the situation is more complex, with CeO_2 contributing to a number of catalytic functions (*50*). In particular it interacts with the noble metal, modifying its reactivity (*50, 51*). In a way these aspects could fit with the selectivity dependence on cerium concentration, BzA increasing almost linearly with it, suggesting that there is an increased supply of lattice oxygen species facilitating oxidation of benzaldehyde further to BzA.

ACKNOWLEDGMENTS

The National Energy Administration and the Swedish Board for Technical Development are acknowledged for financial support.

REFERENCES

1. US Patent, 3,012,043 (1958).
2. Dixon, J. K., and Longfield, J. E., *in* "Catalysis" (P. H. Emmett, Ed.), Vol. VII, p. 266. Reinhold, New York, 1960.
3. Jpn. Kokai, 73, 05739.
4. Czech. Patent, 123106, 148803.
5. Wojtowicz, T., Grzesik, A., Czarnota, T., and Ligeza, A., *Przem. Chem.* **46,** 578 (1961).
6. Andreikov, E. I., and Volkov, V. L., *Kinet. Catal.* **22,** 753 (1981).

7. Slavov, S., Moskovkina M., and Ivanov, K., *Heterog. Catal. Proc. Int. Symp.,* 476 (1987).
8. Inglot, A., Pozmczek, J., and Wenda, E., *Bull. Acad. Pol. Sci. Ser. Sci. Chim.* **28,** 815 (1980).
9. van den Berg, P. J., Brans-Brabant, J. H. L. M., van Dillen, A. J., Flach, J. C., and Geus, J. W., *Ber. Bunsenges. Phys. Chem.* **86,** 43 (1982).
10. Driscoll, R. K., Leupold, E. I., and Herzog, W., *Chem. Ing. Tech.* **59,** 314 (1987).
11. Andreikov, Y. I., Lyapkin, A. A., and Volkov, V. L., *Petrol. Chem. USSR* **17,** 155 (1978).
12. Wu, Y., and Wu, Z., *Cuihua Xuebao* **9,** 210 (1983).
13. Fleury, P., *Rev. Chim. Miner.* **6,** 819 (1969).
14. Wenda, E., *J. Thermal Anal.* **30,** 879 (1985).
15. Volkov, V. L., Fotiev, A. A., Fedotovskikh, N. G., and Andreikov, E. I., *Russ. J. Phys. Chem.* **48,** 887 (1974).
16. Hardy, A., Galy, J., Casalot, A., and Pouchard, M., *Bull. Soc. Chim. Fr.* 1056 (1965).
17. Deschanvres, A., and Raveau, B., C. R. *Acad. Sci. Paris* **259,** 3553 (1964).
18. van Geem, P. C., and Teunissen, A. J. J. M., Neth. Patent Appl., 7,607,598 (1976).
19. Yan, Z.-G., unpublished results.
20. Trion, R., van den Mond, Th., and van den Berg, P. J., *Delft Prog. Rep.* **3,** 263 (1978).
21. Grasselli, R. K., *J. Chem. Educ.* **63,** 216 (1986).
22. Giordano, N., and Bart, J. C. J., *Recl. Trav. Chim. Pays-Bas* **94,** 28 (1975).
23. Otaki, T., Hatano, M., Koyama, T., and Oshima, K., *Jpn Kokai Tokkyo Koho* **79,** 124,885.
24. Ivanov, A. S., Dzis'ko, V. A., Moroz, E. M., and Noskova, S. P., *Kinet. Katal.* **27,** 428 (1986).
25. Engler, B., Koberstein, E., and Schubert, P., *Appl. Catal.* **48,** 71 (1989).
26. Yoshimura, M., and Sata, T., *Bull. Chem. Soc. Jpn.* **42,** 3195 (1969).
27. Andersson, S. L. T., in press.
28. Andersson, S. L. T., *J. Chromatogr. Sci.* **23,** 17 (1985).
29. Niwa, M., and Murakami, Y., *J. Catal.* **76,** 9 (1982).
30. Casalot, A., and Pouchard, M., *Bull. Soc. Chim. Fr.* **10,** 3817 (1967).
31. Fleury, P., and Kohlmuller, F., *Compt. Rend.* **262C,** 475 (1966).
32. Andersson, S., *Acta Chem. Scand.* **19,** 1371 (1965).
33. ASTM, NO. 12-757, US Nat. Bur. Standards, Mono. Vol. 25, Section 1, 1962.
34. Schön, G., *Acta Chem. Scand.* **27,** 2623 (1973).
35. Hammond, J. S., Gaarenstroom, S. W., and Winograd, N., *Anal. Chem.* **47,** 2194 (1975).
36. Nyholm, R., and Mårtensson, N., *J. Phys. Chem.* **13,** L279 (1980).
37. Andersson, S. L. T., *J. Chem. Soc. Faraday Trans. 1* **75,** 1356 (1979).
38. Le Normand, F., El Fallah, J., Hilaire, L., Légaré, P., Kotani, A., and Parlebas, J. C., *Solid State Commun.* **71,** 885 (1989).
39. Germain, J. E., and Laugier, R., *Bull. Soc. Chim. Fr.* 650 (1971).
40. Andersson, S. L. T., *J. Catal.* **98,** 138 (1986).
41. Zhu, J., and Andersson, S. L. T., *J. Catal.* **126,** 92 (1990).
42. Kirk-Othmer, "Encyclopedia of Chemical Technology," Vol. 3, p. 779. Wiley, New York, 1978. 3rd ed.
43. Bachmann, H. G., Ahmed, F. R., and Barnes, W. H., *Z. Kristallogr.* **115,** 110 (1961).
44. Andersson, S. L. T., *J. Chem. Soc. Faraday Trans. 1* **82,** 1537 (1986).
45. Yan, Z.-G., and Andersson, S. L. T., *Appl. Catal.* **66,** 149 (1990).
46. Jonson, B., Rebenstorf, B., Larsson, R., and Andersson, S. L. T., *J. Chem. Soc., Faraday Trans. 1* **84,** 3547 (1988).
47. van den Berg, J. P., Broersma, A., van Dillen, A. J., and Geus, J. W., *Thermochim. Acta* **63,** 123 (1983).
48. Dziembaj, R., *Wiss. Z. Friedrich Schiller Univ. Jena Naturwiss. Reihe* **37,** 819 (1988).
49. Le Normand, F., Bernhardt, P., Hilaire, L., Kili, K. Krill, K., and Maire, G., *Stud. Surf. Sci. Catal.* **30,** 221 (1987).
50. Harrison, B., Diwell, A. F. and Hallett, C., *Platinum Metals Rev.* **32,** 73 (1988).
51. Shyu, J. Z., and Otto, K., *J. Catal.* **115,** 116 (1989).